

Perspective

Affinity Selection in Germinal Centers: Cautionary Tales and New Opportunities

Jose Faro ^{1,2,*}  and Mario Castro ^{3,†} 

¹ Area of Immunology, Faculty of Biology, Biomedical Research Center (CINBIO), Universidade de Vigo, 36310 Vigo, Spain

² Instituto Gulbenkian de Ciência, 2781-901 Oeiras, Portugal

³ Instituto de Investigación Tecnológica (IIT), Grupo Interdisciplinar de Sistemas Complejos (GISC), Universidad Pontificia Comillas, 28015 Madrid, Spain; marioc@comillas.edu

* Correspondence: jfaro@uvigo.es

† Both authors contributed equally to this work.

Abstract: Our current quantitative knowledge of the kinetics of antibody-mediated immunity is partly based on idealized experiments throughout the last decades. However, new experimental techniques often render contradictory quantitative outcomes that shake previously uncontroversial assumptions. This has been the case in the field of T-cell receptors, where recent techniques for measuring the 2-dimensional rate constants of T-cell receptor–ligand interactions exposed results contradictory to those obtained with techniques measuring 3-dimensional interactions. Recently, we have developed a mathematical framework to rationalize those discrepancies, focusing on the proper fine-grained description of the underlying kinetic steps involved in the immune synapse. In this perspective article, we apply this approach to unveil potential blind spots in the case of B-cell receptors (BCR) and to rethink the interactions between B cells and follicular dendritic cells (FDC) during the germinal center (GC) reaction. Also, we elaborate on the concept of “catch bonds” and on the recent observations that B-cell synapses retract and pull antigen generating a “retracting force”, and propose some testable predictions that can lead to future research.

Keywords: antibody-antigen binding; kinetics; mathematical modeling; catch-bond; allostery



Citation: Faro, J.; Castro, M. Affinity Selection in Germinal Centers: Cautionary Tales and New Opportunities. *Cells* **2021**, *10*, 1040. <https://doi.org/10.3390/cells10051040>

Academic Editors:

Michael Meyer-Hermann and
Tanmay Mitra

Received: 12 March 2021

Accepted: 24 April 2021

Published: 28 April 2021

Publisher's Note: MDPI stays neutral with regard to jurisdictional claims in published maps and institutional affiliations.



Copyright: © 2021 by the authors. Licensee MDPI, Basel, Switzerland. This article is an open access article distributed under the terms and conditions of the Creative Commons Attribution (CC BY) license (<https://creativecommons.org/licenses/by/4.0/>).

1. Introduction

The history of Immunology runs in parallel to the use of innovative experimental techniques. From the early microscopes to modern molecular-level sensors, our basic knowledge has been refined through the years; new techniques provide new discoveries. For instance, in 2010 two papers [1,2] revealed essential differences between traditional assays for the interaction of T-cell receptors (TCR) and their peptide-major histocompatibility complex (pMHC) ligands, in which one of the reactants is in fluid phase (referred to as 3-dimensional (3D) assays), and those in which both TCRs and pMHC ligands are confined to a cell membrane (referred to as 2D assays). More recently, an additional layer of complexity was added to the binding kinetics of TCRs with the discovery that some TCRs display a catch-slip bond behavior when they are bound to a given pMHC ligand [3,4]. While the predominant binding of receptors to ligands, known as slip bonds, are characterized by being weakened when a tensile force is applied between the receptor and the ligand, such that the half-life of the bond decreases for increasing tensile force [5,6], in catch bonds the half-life increases for an increase of the tensile force, and catch-slip bonds display initially a catch bond behavior until a threshold value is reached, beyond which the bond becomes a slip one and its half-life decreases for increasing force [6,7]. Typically, the optimum tensile force for TCR-pMHC interactions with catch bond behavior is in the range of 10–20 pN [4], which is within the range of forces per bound TCR generated by pulling in cell–cell interactions [8] and during initial TCR-pMHC binding [9].

Currently, although there is no consensus about the mechanical basis of the catch bond behavior of TCR-pMHC interactions, there is consensus about the role of dimensionality and how different experimental methods can dramatically change previous qualitative and quantitative predictions. In principle, this is how normal science progresses, but when a dominant conceptual paradigm is built based on inappropriate experimental methods it prevents moving the field forward (an illustrative example is the case of the oligoclonal seeding concept in germinal center studies [10,11]). In these cases, mathematical modeling can contribute to unveiling important differences between experimental procedures, to warn against intuitively appealing but wrong interpretations of experimental results and also to suggest new venues to explore [12].

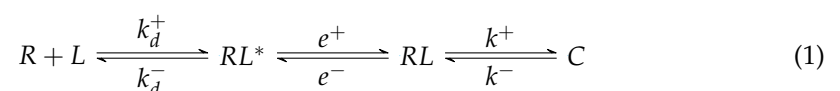
Recently, we have developed a theoretical framework to analyze the effective binding rate constants of TCR-pMHC interactions in 3D and 2D assays [13]. The rationale behind our approach is to disentangle kinetic mechanisms into fine-grained steps. For instance, in that framework binding–unbinding is understood as a sequence of three independent mechanisms—diffusion (translation), orientation (rotation), and molecular binding. Our approach successfully helped to reconcile contradictory experimental results as well as to predict how different experimental assays would lead to divergent predictions [13].

In the case of antibodies (Ab) and the B-cell membrane immunoglobulin (Ig) component of B-cell receptors (BCR), there are also potential pitfalls in interpreting experimental data. As already acknowledged years ago by Mason and Williams [14] the interaction of bivalent Abs to antigen in solution departs considerably from their interaction with cell-bound antigen. Moreover, it has been soundly argued that in real ligand-receptor reactions it is essential to understand the process of events in dynamic cell–cell interactions rather than following equilibrium considerations [15]. This raises the question of how many of the current underlying assumptions on the binding of BCRs to an antigen (Ag) displayed on cell membranes are based on misinterpreted experimental results or on inappropriate extrapolation from *in vitro* fluid phase systems to very different conditions such as cellular systems.

In this perspective article, we apply our theoretical framework to illustrate how it can help to rightly understand and compare binding results of Ab–Ag reactions in solution (3D assays) and in cell–cell interactions during an immune response (2D interactions, as it can be expected *in vivo*). Specifically, we will approach the following two questions: (i) does the dimensionality of the experimental setup impinge in our understanding of interactions of BCRs and Ags held on the membrane of follicular dendritic cells (FDC) during a germinal center (GC) reaction?; (ii) is there a role for catch-bonds in BCR–Ag reactions, and how it could affect Ab affinity maturation in GC reactions?

2. General Theoretical Framework and Derived Properties for Antibody– and BCR–ligand Interactions

Binding and unbinding of ligands (L) to receptors (R) can be described in detail as a series of independent steps (see Figure 1). The first step comprises the spatial approximation of R and L molecules to a distance that allows binding (denoted by RL^*). Once in that state, the two molecules must attain a proper orientation to bind to each other—we denote this intermediate-oriented state as RL —until finally, they can form a complex C [13]. We summarize these series of states and processes in Equation (1), where the translational and rotational diffusion *on* and *off* constant rates correspond either to those in 3D or in 2D settings.



In a deterministic approximation, the general reaction scheme in Equation (1) is described by the system of coupled ordinary differential equations given in Appendix (A1).

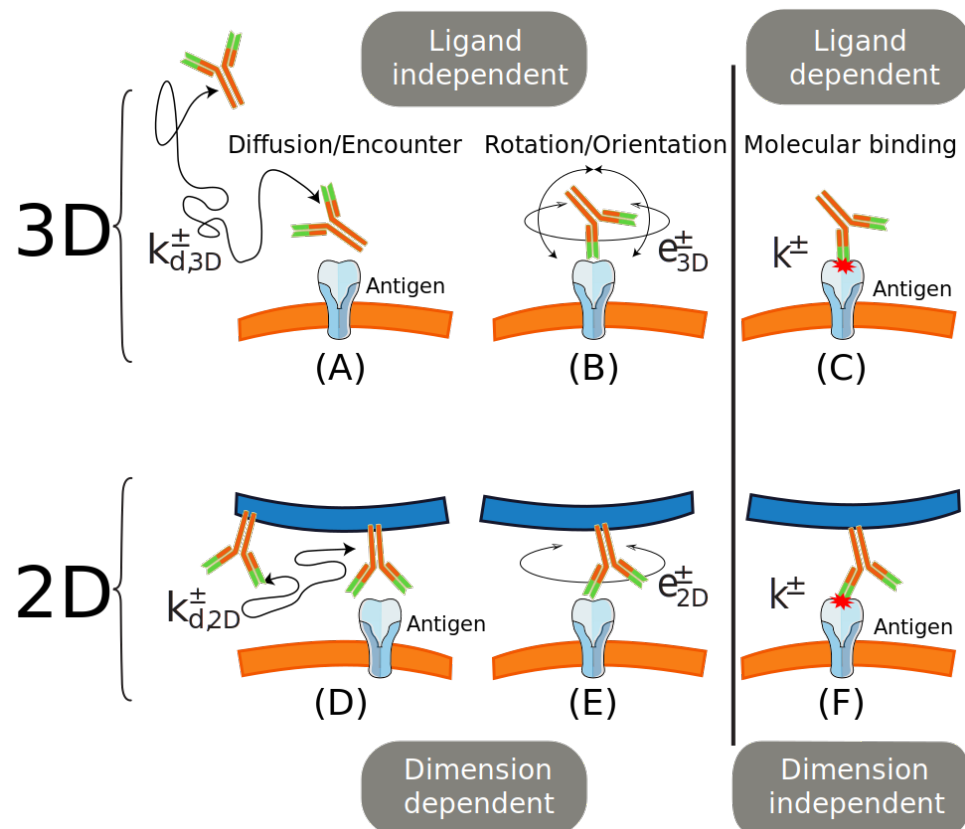


Figure 1. Binding steps in three versus two dimensions. Top row, binding in three dimensions: (A) 3D diffusion/encounter, (B) rotation/orientation, and (C) molecular binding. Bottom row, the three binding steps in two dimensions: (D) 2D (membrane) diffusion/encounter, (E) rotation/orientation, and (F) molecular binding. The vertical line separates dimensional dependent and independent processes.

2.1. Experimentally Estimated Effective on and off Constant Rates

As we have shown previously [13], in the cases of the Surface Plasmon Resonance (SPR, a 3D assay) and the Adhesion Frequency (AF) assay (a 2D assay [1]) Equation (1) is effectively simplified to a single-step description of the process, namely,



where k_{eff}^+ and k_{eff}^- are, respectively, the effective binding and unbinding rate constants. The corresponding system of coupled ordinary differential equations for this simplified global process is:

$$\frac{d[R]}{dt} = \frac{d[L]}{dt} = -k_{\text{eff}}^+[R] \cdot [L] + k_{\text{eff}}^-[C] \tag{3}$$

$$\frac{d[C]}{dt} = k_{\text{eff}}^+[R] \cdot [L] - k_{\text{eff}}^-[C]. \tag{4}$$

This single-step model can be formally derived from Equations (A1a)–(A1d) by assuming a quasi-steady state approximation for the intermediate states $[RL^*]$ and $[RL]$. This means assuming that the time derivatives in Equations (A1b)–(A1c) are in practice equal to zero and solving for $[RL^*]$ and $[RL]$ in terms of the free species ($[R]$ and $[L]$) and the bound complex ($[C]$). Then, after a little algebraic manipulation one arrives (see Appendix A.1, Equations (A2a)–(A3b)), in the case of the SPR and AF assays, to the following expressions for k_{eff}^+ and k_{eff}^- [13]:

$$k_{\text{eff}}^+ = \frac{k_d^+ e^+ k^+}{k_d^- e^- + k^+ (k_d^- + e^+)} \Big|_{3\text{D}/2\text{D}} \tag{5}$$

$$k_{\text{eff}}^- = \frac{k_d^- e^- k^-}{k_d^- e^- + k^+ (k_d^- + e^+)} \Big|_{3\text{D}/2\text{D}}, \tag{6}$$

where the subscripts indicate that the rate constants are those corresponding to either 3D or 2D reactions, and k^+ and k^- are the intrinsic or molecular *on* and *off* constant rates, which are, therefore, identical for the 3D and the 2D interactions.

The effective association affinity constant is simply the product of the affinities (denoted by *capital K*) of every intermediary step:

$$K_A^{\text{eff}} \Big|_{3\text{D}/2\text{D}} \equiv \frac{k_{\text{eff}}^+}{k_{\text{eff}}^-} \Big|_{3\text{D}/2\text{D}} = (K_d K_e)_{3\text{D}/2\text{D}} K_A.$$

When this formalism is applied to Ab–Ag and BCR–Ag interactions it is instructive to plot k_{eff}^+ as a function of k^+ , and k_{eff}^- as a function of k^+ and k^- because it shows how misleading can be the estimation of k^+ and k^- by the effective rate constants k_{eff}^+ and k_{eff}^- , respectively. For instance, according to Equation (5), for Abs and BCRs of the same isotype, when $k^+ \ll \frac{k_d^- e^-}{(k_d^- + e^+)}$ the effective rate k_{eff}^+ will increase linearly for increasing values of k^+ .

However, when k^+ approaches the value $\frac{k_d^- e^-}{(k_d^- + e^+)}$, k_{eff}^+ will increase more and more slowly, approaching asymptotically the maximum $\frac{k_d^+ e^+}{(k_d^- + e^+)}$ when $k^+ \gg \frac{k_d^- e^-}{(k_d^- + e^+)}$ (see Figure 2A). The latter situation could be named diffusion/orientation-limited reactions as the limiting process is not binding itself but getting the Ab or BCR and the Ag close enough and well oriented before the real molecular binding occurs.

With respect to k_{eff}^- , according to Equation (6), when $k^+ \ll \frac{k_d^- e^-}{(k_d^- + e^+)}$ for any given value of k^+ the effective off rate constant is a good estimation of k^- . However, for values of $k^+ \approx \frac{k_d^- e^-}{(k_d^- + e^+)}$ this estimation is not longer valid, and for $k^+ \gg \frac{k_d^- e^-}{(k_d^- + e^+)}$ the value of k_{eff}^- becomes instead a good estimation of the true dissociation constant, more precisely $k_{\text{eff}}^- \propto K_D$ (see Figure 2B). In the remaining of this paper we refer to the quantity $\frac{k_d^- e^-}{(k_d^- + e^+)}$ as the k^+ -threshold.

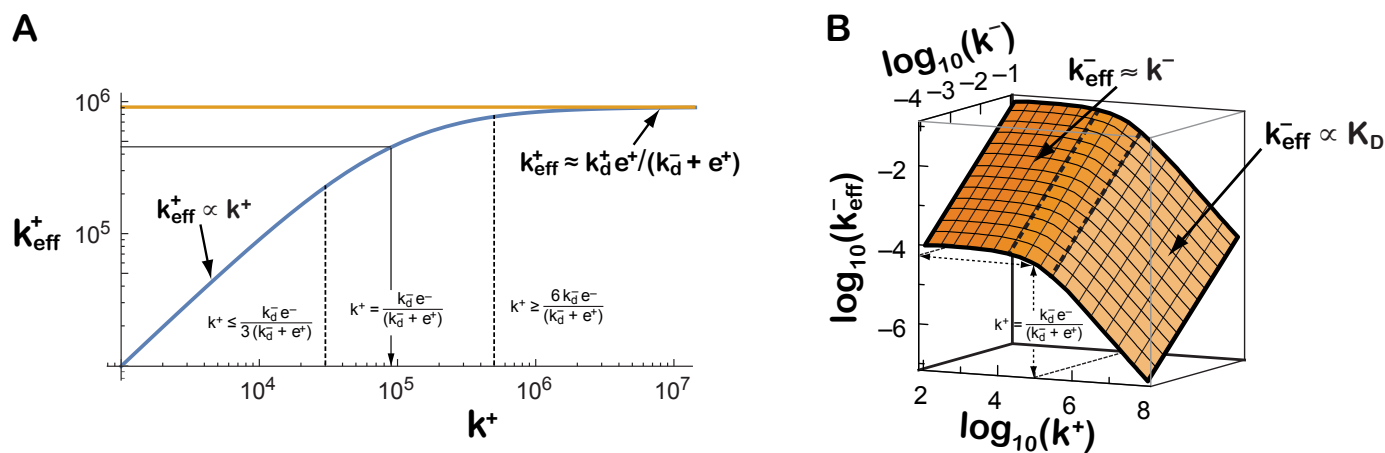


Figure 2. Effective kinetic rates measured experimentally can be misleadingly interpreted as approximations of the underlying molecular binding constant rates. Expected dependency of k_{eff}^+ (panel A) and k_{eff}^- (panel B) as a function of k^+ and k^- , for a given set of values of the translational and rotational rate constants ($k_d^+ = 10^6 \text{ M}^{-1}\text{s}^{-1}$, $k_d^- = 10^3 \text{ s}^{-1}$, $e^+ = 10^4 \text{ s}^{-1}$, $e^- = 10^6 \text{ s}^{-1}$).

In summary, the following approximations hold when k^+ is greater or smaller than $\frac{k_d^- e^-}{k_d^- + e^+}$:

$$(a) \text{ for } k^+ \ll \left(\frac{k_d^- e^-}{k_d^- + e^+}\right)_{3D/2D} : \quad k_{\text{eff}}^+ \approx \frac{k_d^+ e^+}{k_d^- e^-} k^+ = K_d K_e k^+, \quad (7)$$

$$k_{\text{eff}}^- \approx k^-. \quad (8)$$

$$(b) \text{ for } k^+ \gg \left(\frac{k_d^- e^-}{k_d^- + e^+}\right)_{3D/2D} : \quad k_{\text{eff}}^+ \approx \frac{k_d^+ e^+}{(k_d^- + e^+)}, \quad (9)$$

$$k_{\text{eff}}^- \approx \frac{k_d^- e^-}{(k_d^- + e^+)} \frac{k^-}{k^+} = \frac{k_d^- e^-}{(k_d^- + e^+)} K_D. \quad (10)$$

In the following sections we discuss succinctly the mechanisms and geometrical aspects that might raise concerns about our understanding of Ab–Ag and BCR–Ag interactions: diffusion, rotation and dimensionality.

2.2. The Role of Translational Diffusion

Equations (5)–(10) are the roadmap to unveil the differences imposed by geometrical, physical and molecular constraints. In particular, due to geometrical constraints, translational diffusion *on* and *off* constant rates are mathematically different in 2D (membrane) and 3D (solution). Specifically, for unbound BCRs of IgM and IgG isotypes the median translational diffusion constant has been estimated to be [16–18]

$$D_T(2D) = 4 \times 10^{-2} \mu\text{m}^2/\text{s} - 10^{-1} \mu\text{m}^2/\text{s}, \quad (11)$$

and for IgD BCRs $D_T(2D) = 3 \times 10^{-3} \mu\text{m}^2/\text{s}$ [17]. However, for free IgMs and IgGs in diluted saline solutions, as is the case in many SPR experimental setups, $D_T(3D)$ has been reported to be [19–21]

$$D_T(3D) = 10 \mu\text{m}^2/\text{s} - 60 \mu\text{m}^2/\text{s}. \quad (12)$$

In a 2D setting, the translational diffusion *on* rate constant of BCRs toward an Ag tethered on a cell membrane can be approximated by the expression: $k_d^+(2D) = 2\pi D_T / \log(b/s)$ (a clear derivation of it can be found in [22], pp. 151–152, Section 4.2.3) where D_T is the translational diffusion constant of BCRs in the membrane (the contribution to total translational diffusion of Ag tethered on the membrane of a cell like FDCs is very small or none at all), b is the mean distance between BCRs in the membrane of a B cell, and s is the encounter radius, which is essentially the radius of a BCR (~ 7.5 nm [23]). Following Lauffenburger and Linderman (see p. 153 in Reference [22]), to convert $k_d^+(2D)$ into the same unit as a typical bimolecular *on* rate, we multiply by N_A (Avogadro constant) and, to give an estimated local volume for cell surface components, by a membrane thickness of $\ell = 10$ nm. Considering a B cell with a surface area of $40 \mu\text{m}^2$ (corresponding to a diameter of $\sim 7 \mu\text{m}$) and about 50,000 BCRs, it follows $b \approx 28$ nm. Then, using D_T from Equation (11) one finds:

$$k_d^+(2D) = \ell N_A (2\pi D_T / \log(b/s)) = 2.2 \times 10^5 \text{ M}^{-1}\text{s}^{-1} - 2.9 \times 10^6 \text{ M}^{-1}\text{s}^{-1}. \quad (13)$$

The corresponding translational diffusion *off* rate constant can be approximated as:

$$k_d^-(2D) = k_d^+(2D) / (\ell N_A A_c) = 2.1 \times 10^2 \text{ s}^{-1} - 2.7 \times 10^3 \text{ s}^{-1}, \quad (14)$$

where A_c is the effective local cell surface area, defined as $A_c = \pi s^2$ [22].

In 3D, the translational diffusion *on* and *off* rate constants of proteins can be approximated by $k_d^+(3D) = 4\pi D_T s N_A$ and $k_d^-(3D) = 3D_T / s^2$, where s is, as before, the encounter radius [13]. This applied to free IgGs using the estimate in Equation (12) yields:

$$k_d^+(3D) = 3.8 \times 10^8 \text{ M}^{-1}\text{s}^{-1} - 3.4 \times 10^9 \text{ M}^{-1}\text{s}^{-1} \quad \text{and} \quad k_d^-(3D) = 5.3 \times 10^5 \text{ s}^{-1} - 7.2 \times 10^6 \text{ s}^{-1}. \quad (15)$$

2.3. The Role of Rotational Diffusion

Antibodies and BCRs bind to Ags through a small part in the variable region, a small area at the end of each Fab arm known as antigen-binding site or paratope (P). The corresponding region at the surface of the cognate Ag, that is, the actual part of the Ag participating in the Ab–Ag or BCR–Ag bond, is denoted epitope (E).

The spatial position of a BCR Fab paratope is determined by two possible Fab twists and two possible Fab tilts, sketched in Figure 2A,B. The twists are: (1) of a whole BCR relative to the axis along the Fc region, normal to the plasma membrane, denoted here Fc twist rotation, with values in principle in the range $[-360^\circ, +360^\circ]$; and (2) of a Fab arm relative to its major axis (i.e., the hinge–paratope axis), denoted here Fab twist rotation, with values, at least for some Ig isotypes, in the range $[-180^\circ, +180^\circ]$ relative to the more relaxed conformation [24,25].

Similarly, the tilts or wagging and wobbling are: (1) of the whole BCR relative to the major axis of the molecule (along the Fc region, normal to the plasma membrane) denoted here Fc tilt; and (2) of a Fab arm relative to its major axis, denoted here Fab tilt; the range of this tilt is much larger than the Fc tilt range (in some isotypes the angle of the Fab tilt cone may be even larger than 90° [26–28]).

Considering the rotational movements sketched in Figure 3a,b, once a BCR and an Ag are in the RL^* state one can map the binding problem to that of random walk of a paratope on a region of a spherical surface of radius $R = \text{length of a Fab arm} \approx 84 \text{ \AA}$ [23,29] delimited by altitude and azimuthal angles θ and β , respectively, constrained by the flexibility of the hinge of the Fab arm (Figure 3c). Thus, a paratope P diffuses within this restricted spherical surface region until it reaches its cognate epitope E . This epitope can be described as a small area on the mentioned spherical surface covering an arc of maximum length $L \approx 28 \text{ \AA}$ [30], which is equivalent to an angle $\delta \approx 19^\circ$ (Figure 3c). In addition, once the paratope P is close to the epitope E , proper binding requires their proper alignment or orientation through Fab twist rotation, so not only rotational-tilt diffusion to the right location matters, also proper alignment is mandatory (twist or rotational-alignment). Note that, following unbinding the possibility of immediate rebinding is lost when either movement is reversed, namely, the alignment is lost or the Fab paratope P leaves the proximity of the epitope E through tilting diffusion.

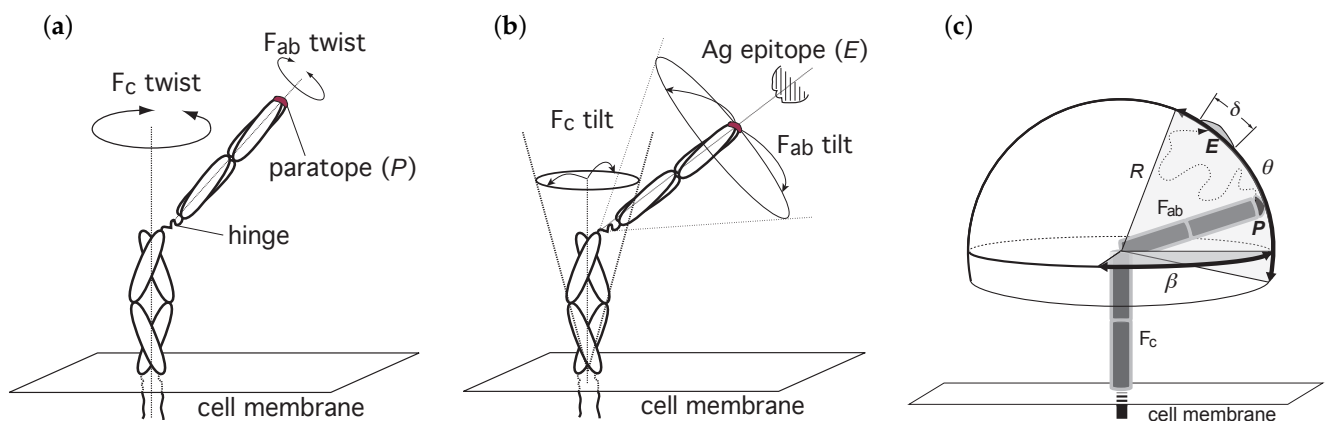


Figure 3. Possible rotations having an impact on the position of a paratope P relative to an Ag epitope E . The position of P in a membrane Ig is submitted to (a) two possible twists, and (b) two possible tilts (wagging and wobbling). In (c) it is shown a sketch of the diffusion of P constrained to a spherical cap on a sphere of radius $R = \text{length of a Fab arm} \approx 84 \text{ \AA}$ [29] and to Fab altitude and azimuth angles θ and β , respectively. Depicted is a possible path followed by paratope P toward epitope E (dotted line). This movement corresponds to Fab tilt in (b). The angle δ corresponds to an arc on the spherical surface equal to the major length of E . For clarity, in all panels the membrane Ig is depicted with only one Fab arm.

The different IgG subclasses in human and mouse have different hinge regions, and this makes them differ substantially in the flexibility and rotation of their Fab arms with

respect to the Fc region (tilt rotation) [31,32]. More specifically, it has been found that human IgG subclasses can be ordered with respect to hinge flexibility between Fab arms (range of Fab-Fab angles), from most to least flexible, as: IgG3 > IgG1 > IgG4 > IgG2 [26]. Also, it has been shown that murine IgG subclasses can be ranked with respect to their Fab arms flexibility as follows: IgG2b > IgG2a > IgG1 > IgG3 [33]. This two orderings turn out to be totally consistent with each other when the reported functional equivalence of murine and human IgG subclasses is considered [34,35]. For instance, murine IgG2b corresponds to human IgG3 [34] and the maximum tilting angle (Fab-Fc angle) reported in the literature is about $\theta \simeq 70^\circ$ for both [26,33]. Similarly, murine IgG1 corresponds to human IgG4 and both have $\theta \simeq 50^\circ$. These differences and their impact on the average speed of the tilt Fab rotation [33], suggest that Ig class switching could alter the effective binding constant rates of BCR–Ag and Ab–Ag interactions because of a concomitant change in their paratope rotational diffusion rate constants.

2.4. The Role of Dimension

Using experimental data on the relaxation times of fluorescent polarization anisotropy of fluorescent probes [33,36], quantitative information on molecular rotational velocity can be obtained. For instance, the mean square angular deviation of a molecule rotating about a given molecule's axis after a time t is given by [37,38]

$$\langle \phi^2 \rangle = 2D_a t \quad (\text{in units rad}^2),$$

where D_a is the corresponding twist (alignment) rotational diffusion constant. On the other hand, the mean rotational correlation time of a molecule rotating about a given molecule's axis, here denoted by $t_{1\text{rad}}$, is the time it takes on average to rotate 1 rad. From these two definitions it follows that for a Fab arm rotating about its major axis (Fab twist) the twist (alignment) diffusion constant is:

$$D_a = \frac{1 \text{ rad}^2}{2 t_{1\text{rad}}}.$$

However, for a Fab arm rotating about the Fc axis with center in the hinge region (Fab tilt) the tilt rotational diffusion constant is [36]:

$$D_t = \frac{1 \text{ rad}^2}{6 t_{1\text{rad}}}.$$

The values of $t_{1\text{rad}}$ corresponding to Fab tilt as well as to Fab twist have been determined for IgG molecules from fluorescent anisotropy experimental data, with IgG molecules both in solution ($t_{1\text{rad}}(3\text{D})$) and attached through the Fc to a large particle ($t_{1\text{rad}}(2\text{D})$) [33,36,39,40]. Based on that data, it can be estimated that the corresponding 3D rotational (tilt+twist) *off* constant rates e^- are at least 3 orders of magnitude faster than those for 3D translational diffusion *off* constant rates k_d^- (Equation (15)). However, in 2D the e^- constant rates are even much faster than the 2D k_d^- constant rates (Equation (14)). Thus, the k^+ -threshold values in 3D and in 2D can differ from each other by several orders of magnitude. This points out, again, the need to carefully estimate these rates in order to properly understand the outcome of different experimental setups.

In general, for Ab–Ag interactions in a typical experiment using SPR (a 3D assay), the translational constant rates and the rotational constant rates will depend on which of the two interacting molecules is immobilized. There are two possibilities: (1) antigens in solution and Abs immobilized, (2) antigens immobilized and Abs in solution. In the first case, the translational constant rates, k_d^+ and k_d^- , will be only slightly different for Ags of widely different sizes and shapes [20], but the rotational diffusion constants D_t and D_a will be very different for Ags of widely different sizes and shapes, and different (but not very different) for Abs of different isotype or subclass. As a consequence, the total rotational diffusion constants (D_t of Ag + D_t of Ab, and D_a of Ag + D_a of Ab) can be very different for different Ags and Abs, and therefore can differ very much in their rotational

rate constants e^+ and e^- . In contrast, in the second case (Ag immobilized, Ab in solution), the translational diffusion constant and the corresponding rate constants, k_d^+ and k_d^- , will be very similar for Abs of different isotypes, because it has been experimentally found that the 3D translational diffusion constant is affected very little, if at all, for a broad range of protein sizes [20], and the rotational rate constants, e^+ and e^- , will be the same for Abs of same isotype and subclass, and different (but not very different) for Abs of different isotype or subclass. Notice that, in this case, irrespective of the mean distance between Ag molecules on the sensor surface, Fab tilting/twist is always involved, either in the Ab binding to an epitope or in preventing immediate rebinding after an unbinding event.

Therefore, according to Equations (5) and (6), the differential contribution of Abs and Ags to the 3D rotational constant rates of Ab–Ag interactions is expected to have an important impact on the effective 3D rate constants, k_{eff}^+ and k_{eff}^- , depending on which of the two interacting molecules, Abs or Ags, is immobilized, a theoretical prediction consistent with experimental observations [41].

However, in 2D reactions, BCRs interact with Ag in form of immune complexes tethered on cell membranes, notably FDCs. These Ag complexes (termed iccosomes [42]) are much larger than BCRs (25 to 50-fold difference in size) and are anchored to the FDC membrane by several receptor molecules, namely, Fc receptors and C3b/C4b receptors [23,42] (Figure 4). Hence, the contribution of Ag complexes to diffusion and rotation are expected to be negligible compared to that of BCRs. Then, for different BCRs and Ags the translational rate constants, k_d^+ and k_d^- , would be similar because BCRs of different isotypes have similar 2D translational diffusion constants [16–18], and the rotational rate constants, e^+ and e^- , would be similar for BCRs of same isotype/subclass, and different (but not very different) for BCRs of different isotype or subclass.

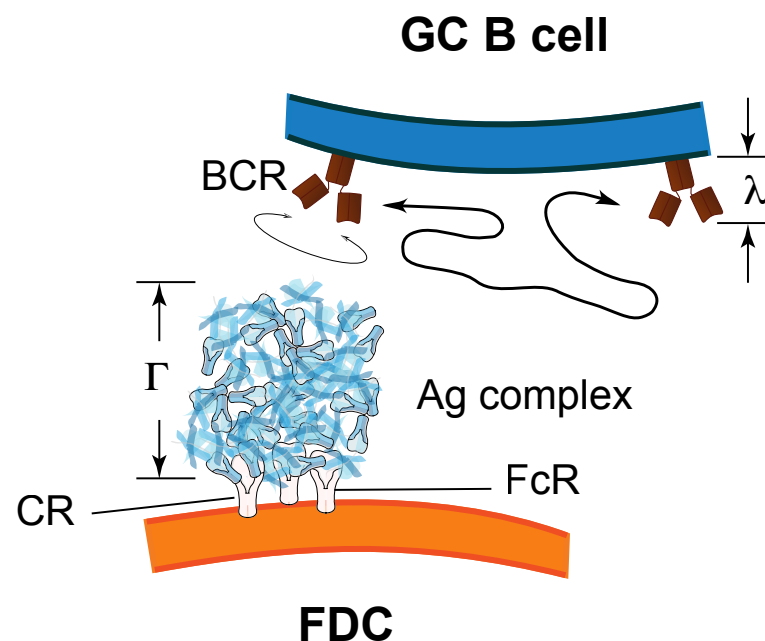


Figure 4. BCRs contribute to translational and rotational diffusion to a much larger extent than Ag complexes on FDCs (termed iccosomes). Iccosomes are tethered to the FDC membrane through several Fc and/or complement receptors. Typical diameter of iccosomes is $\Gamma = 250\text{--}700$ nm [42], while BCR diameter is $\lambda = 10\text{--}15$ nm [23]. FcR, Fc receptor; CR, complement receptor.

All the above indicates that, in general, for Ab–Ag interactions the k^+ -threshold value $\frac{k_d^- e^-}{k_d^- + e^+}$ in 3D assays can vary substantially, particularly for Ags of different size when they are in solution. However, the corresponding k^+ -threshold value in 2D BCR–Ag interactions will be independent of Ag (save for epitope valency) and of BCRs, except for BCRs of

different isotype and subclass, which can have k^+ -threshold values differing by at most one order of magnitude.

3. Is There a Role for Catch-Bonds in BCR–ligand Interactions?

3.1. Evidence for Mechanical Forces in B-Cell Synapses and Their Relationship to Kinetic Rate Constants

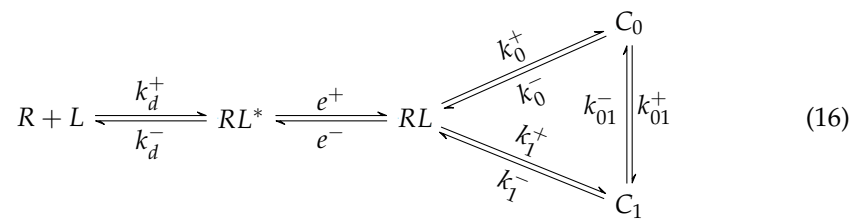
The binding of BCRs to Ag tethered to a plasma membrane induces in B cells the formation of an immune synapse. After the synapse is formed, an initial lateral traction force acts on Ag-bound BCRs, followed by a later retraction that pulls the Ag-bound BCRs [43–45]. The formation of such immune synapses involves an initial clustering of Ag-bound BCRs by an active process, driven intracellularly by myosin, F-actin and dynein [44,46], that generates shear or lateral forces of 10–20 nN per $50 \mu\text{m}^2$ acting on Ag-bound BCRs [46]. Assuming that in that large area there are initially about 10^3 Ag-engaged BCRs, individual BCR–Ag bonds would be submitted to a shear force of 10–20 pN that would increase as the number of broken BCR–Ag bonds increase. The subsequent immune synapse retraction pulls the Ag-bound BCRs, generating a tensile force of 10–20 pN per Ag-bound BCR in the direction normal to the local membrane plane [18,44].

For the process of Ag pulling and extraction, of the three processes and four states distinguished above in BCR–Ag interactions only unbinding and the bound state are relevant. For instance, in order for GC B cells to be able to pull and extract Ag from FDC membrane immune complexes the average time $1/k^-$ has to be large enough compared with the time scale required for the Ag “pulling and extracting” process. This time scale is similar to the time spent by a B cell interacting with a FDC, which has been reported to be on average less than 5 min [47]. Assuming this time is 5 min, $1/k^-$ has to be larger than 300 s, or $k^- < 3 \times 10^{-3} \text{ s}^{-1}$, to allow for Ag extraction. Nevertheless, for larger values of k^- , if compensated for by very large values of k_{eff}^+ , it could still be possible for a B cell to extract Ag.

3.2. An Extension of the Theoretical Framework

It has been shown that some cell–receptor adhesion molecules can be in two different conformational states, the so-called bent and extended states, the second one being favored in receptor–ligand complexes submitted to a tensile force [48]. Also, recently it has been described that TCRs can display dynamic ectodomain allostery [8,49]. Analogously, it has been recently reported that BCRs binding to Ag tethered on a plasma membrane undergo allosteric changes in the CH2 domain, in the B cell membrane-proximal CH domain, as well as in the cytoplasmic tail of IgG BCRs [16,18,50]. Similarly, Ag binding by IgG Abs induced a conformational change in the Fc region of the Abs [51]. Furthermore, a recent analysis of the structure of 15 anti-protein Abs comparing the antigen-bound vs. unbound forms has revealed that the binding process induced in a large fraction of those Abs high allosteric changes in the angle between the variable and the adjacent constant domains in both the heavy and light chains [52]. Finally, it has also been shown using different approaches that the paratope of Abs and BCRs can be at least in two different conformational states [53,54].

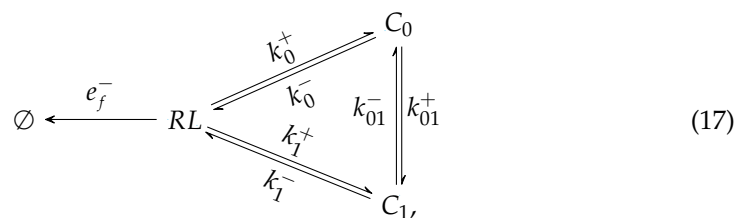
Considering such conformational flexibility of the paratope of BCRs and Abs and the allosteric changes often brought about by antigen binding we assume that in general the complex C in Equation (1) comprise in fact at least two different complex states, C_0 and C_1 , which can be affected allosterically or in some other form by an applied force. Without loss of generality, we assume that in the absence of any applied force the state C_0 is more probable than the state C_1 . Equation (17) summarizes all the states and reactions for most 3D experimental settings in which a free ligand (or receptor) diffuses until it binds to a surface linked receptor (or ligand).



with $k_{01}^+ < k_{01}^-$.

If the Ab class switch induces a dominant conformation swap between the C_0 and C_1 conformations, this can be expressed in terms of Equation (17) as a change in the constant rates k_{01}^+ and k_{01}^- to a new ones, \tilde{k}_{01}^+ and \tilde{k}_{01}^- , respectively, such that $\tilde{k}_{01}^+ > \tilde{k}_{01}^-$. This possibility could have important consequences when considering the effect of lateral and pulling forces on BCR–Ag bonds.

The situation in B cell–FDC interactions and in some experimental 2D settings is slightly different from that shown in Equation (17). For instance, in a variant of the Biomembrane Force Probe (BFP) assay [4] the starting state is a previously bound receptor–ligand complex (either in states C_0 or C_1) that, due to an externally applied tensile force, once the bond is broken, even if the two molecules keep the proper orientation, the probability of rebinding is very low. This experimental setup can be captured more accurately with the following diagram:



where e_f^- and the other rates are constant rates modulated by the applied force.

3.3. Conditions for the Existence of Catch-Slip Bonds in BCR–Ag Interactions

In cell-to-cell experiments using the BFP assay [4], one has $e_f^- > e^-$ and $e^+ = 0$ for $f > 0$. In simple terms, this means that by means of a mechanical procedure, once a BCR unbinds from its ligand the two cell membranes immediately retract from each other. In this case, the interesting observable is the so-called bond survival distribution, $S(t)$, that gives the distribution of empirically observed bond lifetimes at time t under conditions that prevent rebinding. Two time-scales in the distribution $S(t)$ have been experimentally observed so that such bond survival distribution could be fitted phenomenologically to a sum of two exponentials, with weights $0 \leq \omega_1 \leq 1$ and $\omega_2 = 1 - \omega_1$ and respective rates k_1 and k_2 [55]. As shown in Appendix A.2, Equation (A4), this empirical result can be formally derived assuming that the bond survival distribution is a quasi-stationary distribution [56]. Thus, the survival distribution is given by:

$$S(t) \equiv \tilde{p}_0(t) + \tilde{p}_1(t) = \omega e^{-k_1 t} + (1 - \omega) e^{-k_2 t}, \quad (18)$$

with

$$k_1 = \frac{1}{2}(k_{tot} + \kappa) \quad (19)$$

$$k_2 = \frac{1}{2}(k_{tot} - \kappa) \quad (20)$$

$$\omega = \frac{1}{2} + \frac{(1 - 2\alpha)(k_1^- - k_0^-) + k_{01}^- + k_{01}^+}{2\kappa}, \quad (21)$$

where

$$\text{(Total kinetic rate)} \quad k_{\text{tot}} = k_1 + k_2 = k_1^- + k_0^- + k_{01}^- + k_{01}^+ \quad (22)$$

$$\begin{aligned} \text{(Kinetic rate difference)} \quad \kappa &= k_1 - k_2 = \sqrt{k_{\text{tot}}^2 - 4(k_1^-(k_0^- + k_{01}^+) + k_0^- k_{01}^-)} \\ &= \sqrt{(k_1^- - k_0^- + k_{01}^- - k_{01}^+)^2 + 4k_{01}^- k_{01}^+} < k_{\text{tot}} \end{aligned} \quad (23)$$

and α and $(1-\alpha)$ are the initial occupancy probabilities, respectively, of states C_1 and C_0 . From Equations (A7)–(A8) in Appendix A.2, it turns out that α boils down to the simple expression:

$$\alpha = \frac{k_{01}^+}{k_{01}^- + k_{01}^+}. \quad (24)$$

The importance of Equations (18)–(24) is that they allow us to explore the effect of the force on the bond survival distribution $S(t)$. Specifically, if the bond kinetics is understood under an allosteric model where the kinetic rates depend on the free-energy landscape containing the work done by the applied force f , then, in our notation, one has [48]:

$$k_0^-(f) = k_0^-(0) \exp\left(\frac{fx_0}{k_B T}\right) \quad k_1^-(f) = k_1^-(0) \exp\left(\frac{fx_1}{k_B T}\right) \quad (25)$$

and

$$k_{01}^+(f) = k_{01}^+(0) \exp\left(\frac{fx_{01}}{k_B T}\right) \quad k_{01}^-(f) = k_{01}^-(0) \exp\left(\frac{-fx_{10}}{k_B T}\right), \quad (26)$$

where k_B is the Boltzmann constant, T is the absolute temperature of the system, and x_0 and x_1 are the distances from the minima of the receptor–ligand complex potential energy, respectively, in the C_0 and the C_1 states to the maximum of the potential energy that acts as a barrier between the bound and the unbound (RL) states. Similarly, x_{01} and x_{10} in Equation (26) represent the distances or widths from the minima in the C_0 and C_1 states, respectively, to the maximum of the potential energy between both states.

Equations (25) and (26) summarize the changes produced by the force in the free energy landscape relating states RL , C_0 and C_1 in Equation (17). Note that the effect of the force is different on each rate and this can explain why some systems display catch-bond behavior while others do not. Nevertheless, this outcome depends on how k_1 , k_2 and ω change with the applied force. More concretely, note that the relative weight of each timescale in Equation (18) (quantified by ω) would also depend on the applied force. This effect might be observed experimentally because the expected time t_x at which the survival function transitions from one timescale to the other depends on κ and ω and, hence, indirectly on the applied force f . This can be easily seen by considering that the time t_x is determined by the condition $\omega e^{-k_1 t_x} = (1-\omega)e^{-k_2 t_x}$, which yields after some algebraic manipulation:

$$t_x = \frac{1}{\kappa(f)} \left| \ln \left(\frac{1-\omega(f)}{\omega(f)} \right) \right|, \quad (27)$$

where $\kappa = k_1 - k_2$. Note that t_x does only exist for force values at which $\omega(f) \geq 1/2$. Interestingly, some recent studies suggest that at least at $f = 0$ the transition rates between C_0 and C_1 are faster than the unbinding rates into RL [54], that is,

$$k_{01}^+, k_{01}^- \gg k_0^-, k_1^-. \quad (28)$$

If all the distances in Equations (25) and (26) are within the same order of magnitude, namely, $x_0 \simeq x_1 \simeq x_{10} \simeq x_{01} \equiv x$, then for $f > 0$ the above relationships still hold and $|(1-2\alpha)(k_1^- - k_0^-)| \ll k_{01}^+ + k_{01}^-$, and hence Equation (21) can be approximated by:

$$\omega \simeq \frac{1}{2} + \frac{k_{01}^- + k_{01}^+}{2\kappa} > \frac{1}{2}.$$

In general, the system's response to the force will be determined by the sensitivity of the parameters with respect to the applied force. The sensitivity $\sigma_X(f)$, of the variable X with respect to f [57,58] is defined as:

$$\sigma_X(f) = \frac{\partial X}{\partial f}.$$

Applying this to the rates in Equations (25) and (26) we find that

$$\sigma_{k_{01}^-}(f) < 0, \quad \sigma_{k_{01}^+}(f), \sigma_{k_0^-}(f), \sigma_{k_1^-}(f) > 0.$$

From Equation (24), and taking into account that for $f = 0$ the state C_0 is more favorable, it follows that $\alpha(0) < 1/2$ and therefore $k_{01}^-(0) > k_{01}^+(0)$. Hence, we can assume the following hierarchy of kinetic rates

$$k_{01}^-(0) > k_{01}^+(0) \gg k_0^-, k_1^-. \quad (29)$$

This means that, for small forces, the (negative) sensitivity of k_{01}^- will dominate for lower values of the force—as we expect that, roughly, all the distances in Equations (25) and (26) (x_0, x_1, x_{01} and x_{10}) are of the same order. Also, taking into account our previous discussion, it is plausible that $k_{01}^-(0) > k_{01}^+(0) + k_0^- + k_1^-$.

Under these reasonable conditions, we can conclude that,

$$\begin{cases} \sigma_{k_{\text{tot}}}(f), \sigma_{\kappa}(f), \sigma_{\omega}(f) < 0 & \text{for small } f, \\ \sigma_{k_{\text{tot}}}(f), \sigma_{\kappa}(f), \sigma_{\omega}(f) > 0 & \text{for large } f, \end{cases} \quad (30)$$

which provides a mechanism for the qualitative behavior of the survival function defined in Equation (18). This situation is depicted schematically in Figure 5.

This change in the qualitative behavior of the survival function with force has been observed in platelet adhesion [55], and therefore it is sensible to experimentally test it in BCR–Ag interactions. If observed, it would support the idea that the BCR–Ag interactions are subject to force-dependent kinetic rates and also would help to estimate x_{01} and x_{10} in Equation (26).

Equation (18) also allows us to explore the dependence of the mean bond duration and the applied force. Note that the probability density of the bound state as a whole ($C_0 + C_1$) is given by,

$$p(t) = -\frac{dS}{dt},$$

so the mean bond duration is simply

$$\tau(f) \equiv \int_0^{\infty} tp(t)dt = \int_0^{\infty} -tS'(t)dt = -[tS]_0^{\infty} + \int_0^{\infty} S(t)dt = \frac{\omega(f)}{k_1(f)} + \frac{1-\omega(f)}{k_2(f)}. \quad (31)$$

From this expression, it is straightforward to show that

$$\sigma_{\tau}(f) \equiv \frac{d\tau(f)}{df} = -\left|\frac{1}{k_2} - \frac{1}{k_1}\right| \sigma_{\omega}(f) - \left|\frac{\omega}{k_1^2}\right| \sigma_{k_1}(f) - \left|\frac{(1-\omega)}{k_2^2}\right| \sigma_{k_2}(f). \quad (32)$$

Hence, the sensitivity of the mean time is the sum of negative *weights* times the sensitivities of ω, k_1 and k_2 .

As we discussed above, it is plausible that all the distances (x_0, x_1, \dots) in Equations (25) and (26) are of the same order of magnitude. Although this is not necessary for our discussion, it simplifies greatly the mathematical results and highlights the relevance of different parameters. For instance, we can define a scaled force, $fx/k_B T$, such that the timescales k_1 and k_2 , their respective weights ω and $(1-\omega)$, and the mean binding time τ can display non-monotonic behavior, as shown in Figure 5. In particular, note how $\tau(f)$ would increase for small values of the (scaled) force—catch bond behavior—and later it would decrease—slip bond behavior.

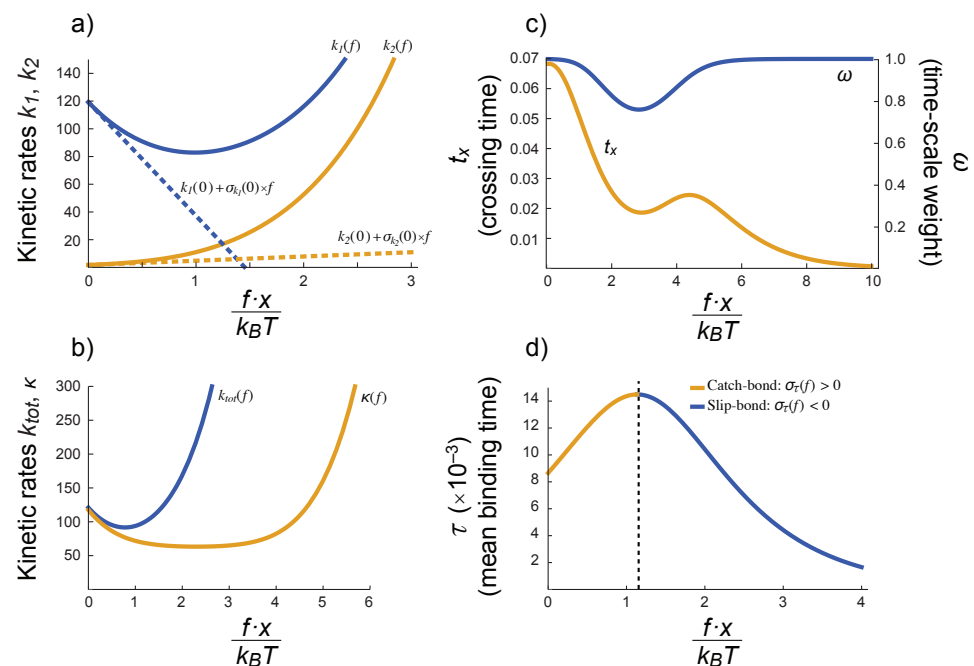


Figure 5. The BCR–Ag interaction might display a catch-bond behavior. The dependence on the force f of the main kinetic rates k_1 and k_2 (defined in Equations (19) and (20)), the rates k_{tot} and κ (defined in Equations (22) and (23)), timescales weight ω (defined in Equation (21)), and times t_x and τ (defined in Equations (27) and (31)) is introduced in those variables through the basic rates k_0^-, k_1^-, k_{01}^+ and k_{01}^- defined in Equations (25) and (26). (a) Variation of k_1 and k_2 with the (scaled) applied force; dashed lines are the corresponding tangent lines at $f = 0$ with slopes equal to the rates sensitivities at $f = 0$. Note how the negative sensitivity of $k_{01}^-(f)$ affects the sign of the sensitivity of k_1 and k_2 at low forces. (b) Total kinetic rate, k_{tot} and kinetic rates difference, κ . (c) Weight of the timescales, ω , and crossing time, t_x . (d) Dependence of the mean bond lifetime, τ , on the (scaled) applied force. The combination of k_1 , k_2 and ω in Equation (31) and the negative sensitivity of $k_{01}^-(f)$ opens the possibility of a catch-bond behavior (the binding time increases with the applied force, at least for low forces). These plots were obtained using the following parameter values: $k_{01}^-(0) = 100$, $k_1^-(0) = 10$, $k_0^-(0) = 1$, $k_{01}^+(0) = 10$, and assuming $x_0 = x_1 = x_{01} = x_{10}$.

This deserves a more thorough exploration (qualitative and quantitative) when experimental data become available, but it is out of the scope of this Perspective article. However, it is worth emphasizing that a role for catch-bonds in BCR–ligand interactions is clearly an open and not unlikely possibility.

4. Discussion

We have argued here that Ab–Ag binding constant rates measurements, both 3D and 2D, are effective estimations that may be not even proportional to the intrinsic binding rates. We have also shown that effective estimations of 3D constant rates may be not proportional to the effective 2D constant rates and, hence, they can be misleading when used to interpret results involving 2D BCR–Ag interactions, particularly BCR-driven B-cell activation and/or Ag endocytosis.

Moreover, irrespective of the effect different isotype glycosylations may have on the constant rates of Abs and BCRs [29], we have clarified here that Ig class switching might significantly alter the effective binding constant rates of BCR–Ag and Ab–Ag interactions, mainly because of the concomitant change in the rotational diffusion rate constants. This is particularly relevant for interpreting correctly—in terms of Ab affinity maturation—the k_{eff}^+ and k_{eff}^- of BCRs and secreted Abs, respectively, of GC B cells and plasmablasts that have undergone class switch. In the case of secreted Abs, $k_{\text{eff}}^+(3\text{D})$ and $k_{\text{eff}}^-(3\text{D})$ are often obtained with the SPR technique, and are used as surrogates of k^+ and k^- , respectively.

According to what was discussed in Section 2.4 with respect to 3D Ab–Ag interactions, there are two main, opposite possible effects of class switch: (1) an increase of the 3D k^+ -threshold $\left(\frac{k_d^- e^-}{k_d^- + e^+}\right)_{3D}$, and (2) a decrease of the 3D k^+ -threshold. In the first situation, if the increase is significant, for instance, when a class switched Ab decreases $e^+(3D)$ 6-fold, and increases $e^-(3D)$ 3-fold, in which case the 3D k^+ -threshold will increase 8-fold, this increase will cause in the class switched Ab a decrease of the effective constant rate $k_{\text{eff}}^+(3D)$ and an increase of $k_{\text{eff}}^-(3D)$ with respect to the corresponding values of the Ab before its switch (see Appendix A.3), in spite of the fact that the two Abs have the same variable region. If such class-switched Ab gets later a mutation causing an increase of k^+ and/or a decrease of k^- , this could be detected by SPR as an increase of $k_{\text{eff}}^+(3D)$ or a decrease of $k_{\text{eff}}^-(3D)$, respectively, with respect to the unmutated Ab. In other words, an Ab class switch that causes an increase of the 3D k^+ -threshold may allow detecting mutation-driven affinity maturation of class switched Abs. In the second case (class switch causes a decrease of the 3D k^+ -threshold) there would be a corresponding increase of $k_{\text{eff}}^+(3D)$ and decrease of $k_{\text{eff}}^-(3D)$. In this case, since $k_{\text{eff}}^+(3D)$ will get closer to the $k_{\text{eff}}^+(3D)$ plateau (see Figure 2), a mutation-driven increase of k^+ could be barely detected or not at all by the SPR technique in the corresponding secreted Abs, and the concomitant decrease of $k_{\text{eff}}^-(3D)$ could not correspond to a decrease of k^- , but to a decrease of the affinity dissociation constant K_D .

In contrast, in 2D BCR–Ag interactions, not only Ag barely contributes to translational and rotational diffusion in 2D BCR–Ag interactions (discussed toward the end of Section 2.4), but solely the IgD to IgG class switch impacts significantly the translational diffusion rate constants $k_d^+(2D)$ and $k_d^-(2D)$ (nearly 10-fold variation; see Section 2.2) as well as the 2D rotational diffusion constants [28]. Thus, a BCR class switch from IgD to IgG1 can increase the k^+ -threshold $\left(\frac{k_d^- e^-}{k_d^- + e^+}\right)_{2D}$ by 8–10-fold. However, other BCR class switches will affect only the BCR rotational diffusion constant rates $e^+(2D)$ and $e^-(2D)$, and since in general $k_d^-(2D) \ll e^+(2D)$, we expect the corresponding change in k^+ -threshold to be small as shown in the following. Let us take for $k_d^-(2D)$ the upper bound $k_d^-(2D) = 2.7 \times 10^3 \text{ s}^{-1}$, and consider a BCR with $e_{2D}^+ = 1.3 \times 10^6 \text{ s}^{-1}$ and $e_{2D}^- = 4.4 \times 10^9 \text{ s}^{-1}$. A BCR class switch from IgG1 to IgG2b can lead to a 2-fold increase in D_t , a 1.5-fold increase in D_a and a 1.5 increase in the tilt angle θ , which implies a 3-fold increase in $e^+(2D)$ and a 1.6-fold increase in $e^-(2D)$. A simple calculation shows then that the k^+ -threshold would decrease from $8.8 \times 10^6 \text{ s}^{-1}$ to $4.8 \times 10^6 \text{ s}^{-1}$, which is less than a 2-fold change. Therefore, whether $k^+ \ll 2D$ k^+ -threshold or $k^+ \gg 2D$ k^+ -threshold before a BCR switch, that condition will likely persist after switching. This predicts that estimations of $k_{\text{eff}}^+(2D)$ and $k_{\text{eff}}^-(2D)$ will not depend on the BCR isotype, except for a switch from BCR IgD. Moreover, whether $k_{\text{eff}}^+(2D)$ and $k_{\text{eff}}^-(2D)$ are good estimators, respectively, of k^+ and k^- will depend on whether k^+ is larger or smaller than the 2D k^+ -threshold before class switch (except when the switch is from IgD).

When GC B cells bind an Ag presented by FDCs they form an immune synapse that later retracts, pulling the BCR-bound Ag. This Ag pulling, when successful, ends up creating an endosomal vesicle containing the extracted material [43,45,59,60]. If the multivalent binding of immune complexes to Fc and complement receptors on FDCs is stronger than the rupture force of FDC membrane integrity nearby those immune complexes, then it can be expected that, in general, the tensile force either breaks the BCR–Ag bond or it extracts bites of the FDC membrane, including immune complexes plus Fc and complement receptors. Otherwise, the tensile force will lead either to a break of the BCR–Ag bond or to extract only immune complexes. In principle, the force generated by this Ag pulling can modify the BCR–Ag bond strength either decreasing it (*slip*-bond), or first increasing it and then decreasing it for increasing forces (*catch-slip* bond) [4,61]. Some recent observations lend support to this second possibility [43,50,62]. In this later case, the increased force resistance can reach the point at which a large Ag extraction takes place. Moreover, increasing the lifetime of a bond when a tensile force is applied could facilitate extracting bites of the antigen presenting cell membrane together with Ag complex. Indeed, this has been recently

reported for B cells [43], reminiscent of an older report that showed how T cells can extract and internalize cognate pMHC molecules from antigen presenting cells [63].

During a moderate Ag extraction most of the engulfed material would be BCR–Ag complexes. Once processed in the endocytic vesicles, they will generate a large fraction of Ag-derived peptides, which will be presented to follicular T helper (Tfh) cells in form of peptide-MHC class II (MHCII) molecular complexes. In contrast, a strong Ag extraction would likely include portions of the FDC membrane [43,47], recruiting irrelevant proteins together with BCR–Ag complexes into the same endocytic vesicle. During the ensuing proteolysis in the endocytic vesicles a plethora of different peptides will be generated, many of them derived from FDC-membrane self-proteins, effectively diluting Ag-derived peptides in the vesicle. Consequently, the number of MHCII molecules presenting Ag-derived peptides would decrease. This implies that a B cell with high-affinity BCRs that bind Ag with slip bonds can present as many Ag-derived peptides as a B cell with moderate-affinity BCRs that bind Ag with catch bonds. Conversely, B cells with high-affinity BCRs that bind Ag with catch bonds can present as many Ag-derived peptides or even less than B cells with moderate-affinity BCRs that bind Ag with slip bonds, thus setting an effective trade-off to the strength of BCR–Ag bonds.

In summary, given the evidence supporting the existence of Ig allosteric states [16,52–54], we have shown here that under very broad conditions for the kinetic rates there is ample room for the existence of catch bonds in BCR–Ag interactions. If that is the case, then it could be expected that there would be some optimum BCR–Ag affinity for best Ag-derived p-MHCII presentation to Tfh cells. Moreover, if different BCRs with specificity for the same Ag differ in their bond properties (slip vs. catch), then this property could be a selectable trait in GCs, favoring both high-affinity BCRs with slip bonding and moderate-affinity BCRs with catch bonding. So far, the immunological relevance of this possibility is unclear but the technology to confirm its existence is already available.

Author Contributions: All authors contributed equally to this work. All authors have read and agreed to the published version of the manuscript.

Funding: This research has been funded by the Spanish Ministerio de Ciencia, Innovación y Universidades-FEDER funds of the European Union support, under project PID2019-106339GB-I00, and by Xunta de Galiza under project GRC-ED431C 2020/02.

Institutional Review Board Statement: Not applicable.

Informed Consent Statement: Not applicable.

Data Availability Statement: Not applicable.

Acknowledgments: The authors thank Emilio Faro for his help in clarifying some equations.

Conflicts of Interest: The authors declare no conflict of interest.

Abbreviations

The following abbreviations are used in this manuscript:

AF	Adhesion Frequency
BCR	B-cell receptor
BFP	Biomembrane Force Probe
FDC	Follicular dendritic cell
GC	Germinal center
SPR	Surface Plasmon Resonance
TCR	T-cell receptor

Appendix A. Some Mathematical Results

Appendix A.1. Full Model for the General Reaction Scheme

The following system of coupled ordinary differential equations describes the reactions in Equation (1):

$$\frac{d[R]}{dt} = \frac{d[L]}{dt} = -k_d^+[R] \cdot [L] + k_d^-[RL^*], \quad (\text{A1a})$$

$$\frac{d[RL^*]}{dt} = k_d^+[R] \cdot [L] - k_d^-[RL^*] - e^+[RL^*] + e^-[RL], \quad (\text{A1b})$$

$$\frac{d[RL]}{dt} = e^+[RL^*] - e^-[RL] - k^+[RL] + k^-[C], \quad (\text{A1c})$$

$$\frac{d[C]}{dt} = k^+[RL] - k^-[C], \quad (\text{A1d})$$

where the square brackets represent the concentration of the different molecular species.

When the rotational constant rates are large, the time derivatives in Equations (A1b) and (A1c) can be dropped and the *slaved* concentrations $[RL^*]$ and $[RL]$ can be expressed in terms of the remaining ones [13]:

$$[RL^*] = \frac{k_d^+(e^- + k^+)}{e^-k_d^- + k^+(e^+ + k_d^-)} [R] \cdot [L] + \frac{e^-k^-}{e^-k_d^- + k^+(e^+ + k_d^-)} [C] \quad (\text{A2a})$$

$$[RL] = \frac{e^+k_d^+}{e^-k_d^- + k^+(e^+ + k_d^-)} [R] \cdot [L] + \frac{k^-(e^+ + k_d^-)}{e^-k_d^- + k^+(e^+ + k_d^-)} [C] \quad (\text{A2b})$$

Finally, substituting $[RL^*]$ and $[RL]$ into Equations (A1a) and (A1d) yields:

$$\frac{d[R]}{dt} = \frac{d[L]}{dt} = -\frac{k_d^+e^+k^+}{k_d^-e^- + k^+(k_d^- + e^+)} [R] \cdot [L] + \frac{k_d^-e^-k^-}{k_d^-e^- + k^+(k_d^- + e^+)} [C], \quad (\text{A3a})$$

$$\frac{d[C]}{dt} = \frac{k_d^+e^+k^+}{k_d^-e^- + k^+(k_d^- + e^+)} [R] \cdot [L] - \frac{k_d^-e^-k^-}{k_d^-e^- + k^+(k_d^- + e^+)} [C]. \quad (\text{A3b})$$

This model corresponds to the single-step model in which the effective rates are given by Equations (5) and (6).

Appendix A.2. Master Equations

The stochastic dynamics of Equation (17) is captured by the solution of the system of differential master equations:

$$\begin{cases} \frac{dp_\emptyset}{dt} = e_f^- p_{RL} \\ \frac{dp_{RL}}{dt} = k_1^- p_1 + k_0^- p_0 - p_{RL}(k_1^+ + k_0^+ + e_f^-) \\ \frac{dp_0}{dt} = k_{01}^- p_1 + k_0^+ p_{RL} - p_0(k_0^- + k_{01}^+) \\ \frac{dp_1}{dt} = k_1^+ p_{RL} + k_{01}^+ p_0 - p_1(k_1^- + k_{01}^-) \end{cases} \quad (\text{A4})$$

with $p_\emptyset(t) + p_0(t) + p_1(t) + p_{RL}(t) = 1$. Note that the system of Equation (A4) includes an irreversible state (so that $\lim_{t \rightarrow \infty} p_\emptyset = 1$).

The bond survival distribution can be computed as the probability of being in any state C_0 or C_1 conditioned to eventual decay into RL, respectively, $\tilde{p}_0(t)$ and $\tilde{p}_1(t)$:

$$\tilde{p}_0(t) \equiv \frac{p_0(t)}{1 - p_\emptyset(t) - p_{RL}(t)}, \quad \tilde{p}_1(t) \equiv \frac{p_1(t)}{1 - p_\emptyset(t) - p_{RL}(t)}. \quad (\text{A5})$$

Thus,

$$\begin{cases} \frac{d\tilde{p}_0}{dt} = k_{01}^- \tilde{p}_1 - \tilde{p}_0(k_0^- + k_{01}^+) \\ \frac{d\tilde{p}_1}{dt} = k_{01}^+ \tilde{p}_0 - \tilde{p}_1(k_1^- + k_{01}^-) \\ \tilde{p}_0(0) = 1 - \alpha \\ \tilde{p}_1(0) = \alpha \end{cases} \quad (\text{A6})$$

The solution to Equation (A6) is summarized in Equation (18).

The initial condition α is the relative occupancy of state C_1 at $t = 0$, so that from Equations (17) and (A4) and assuming C_0 and C_1 are in quasi-steady state,

$$\alpha \equiv \tilde{p}_1(0) = \frac{k_0^- k_1^+ + (k_1^+ + k_0^+) k_{01}^+}{k_0^- k_1^+ + k_1^- k_0^+ + (k_1^+ + k_0^+) (k_{01}^- + k_{01}^+)} \quad (\text{A7})$$

Assuming also that the reactions in Equation (17) obey *detailed-balance* [22,64], namely,

$$\frac{k_0^+ k_{01}^+}{k_0^- k_{01}^-} = \frac{k_1^+}{k_1^-}, \quad (\text{A8})$$

then we arrive at Equation (24).

Appendix A.3. Effect of k^+ -Threshold Increase (or Decrease) on k_{eff}^+ and k_{eff}^-

In general, given a ratio $\frac{ax}{a+x}$ and a parameter b , with $a, x, b > 0$, one has:

$$\begin{aligned} \frac{ax}{a+x} &< \frac{abx}{ab+x} && \text{for } b > 1 \\ \frac{ax}{a+x} &> \frac{abx}{ab+x} && \text{for } b < 1 \end{aligned}$$

Given the equations:

$$\begin{aligned} k_{\text{eff}}^+ &= \frac{k_d^+ e^+ k^+}{k_d^- e^- + k^+ (k_d^- + e^+)} \\ k_{\text{eff}}^- &= \frac{k_d^- e^- k^-}{k_d^- e^- + k^+ (k_d^- + e^+)} \end{aligned}$$

and considering that $e^+(2D) \gg k_d^-(2D)$ they can be re-written as:

$$\begin{aligned} k_{\text{eff}}^+ &= \frac{k_d^+ e^+ k^+}{\left(\frac{k_d^- e^-}{k_d^- + e^+} + k^+\right) (k_d^- + e^+)} \approx \frac{k_d^+ k^+}{\left(\frac{k_d^- e^-}{k_d^- + e^+}\right) + k^+} \\ k_{\text{eff}}^- &= \frac{\left(\frac{k_d^- e^-}{k_d^- + e^+}\right) k^-}{\left(\frac{k_d^- e^-}{k_d^- + e^+}\right) + k^+} \end{aligned}$$

therefore, if $\frac{k_d^- e^-}{k_d^- + e^+}$ increases then k_{eff}^+ decreases and k_{eff}^- increases, and vice versa.

References

- Huang, J.; Zarnitsyna, V.; Liu, B.; Edwards, L.; Jiang, N.; Evavold, B.; Zhu, C. The kinetics of two dimensional TCR and pMHC interactions determine T cell responsiveness. *Nature* **2010**, *464*, 932. [[CrossRef](#)]
- Huppa, J.; Axmann, M.; Mörtelmaier, M.; Lillemeier, B.; Newell, E.; Brameshuber, M.; Klein, L.; Schütz, G.; Davis, M. TCR-peptide-MHC interactions in situ show accelerated kinetics and increased affinity. *Nature* **2010**, *463*, 963–967. [[CrossRef](#)] [[PubMed](#)]
- Kim, S.T.; Shin, Y.; Brazin, K.; Mallis, R.J.; Sun, Z.Y.J.; Wagner, G.; Lang, M.J.; Reinherz, E.L. TCR Mechanobiology: Torques and Tunable Structures Linked to Early T Cell Signaling. *Front. Immunol.* **2012**, *3*, 76. [[CrossRef](#)] [[PubMed](#)]

4. Liu, B.; Chen, W.; Evavold, B.D.; Zhu, C. Accumulation of dynamic catch bonds between TCR and agonist peptide-MHC triggers T cell signaling. *Cell* **2014**, *157*, 357–368. [CrossRef] [PubMed]
5. Bell, G.I. Models for the specific adhesion of cells to cells. *Science* **1978**, *200*, 618–627. [CrossRef]
6. Dembo, M.; Torney, D.C.; Saxman, K.; Hammer, D.A. The reaction-limited kinetics of membrane-to-surface adhesion and detachment. *Proc. R. Soc. Lond. Ser. Biol.* **1988**, *234*, 55–83. [CrossRef]
7. Marshall, B.T.; Long, M.; Piper, J.W.; Yago, T.; McEver, R.P.; Zhu, C. Direct observation of catch bonds involving cell-adhesion molecules. *Nature* **2003**, *423*, 190–193. [CrossRef] [PubMed]
8. Hwang, W.; Mallis, R.J.; Lang, M.J.; Reinherz, E.L. The $\alpha\beta$ TCR mechanosensor exploits dynamic ectodomain allostery to optimize its ligand recognition site. *Proc. Natl. Acad. Sci. USA* **2020**, *117*, 21336–21345. [CrossRef]
9. Liu, Y.; Blanchfield, L.; Ma, V.P.Y.; Andargachew, R.; Galior, K.; Liu, Z.; Evavold, B.; Salaita, K. DNA-based nanoparticle tension sensors reveal that T-cell receptors transmit defined pN forces to their antigens for enhanced fidelity. *Proc. Natl. Acad. Sci. USA* **2016**, *113*, 5610–5615. [CrossRef]
10. Faro, J.; Or-Guil, M. How oligoclonal are germinal centers? A new method for estimating clonal diversity from immunohistological sections. *BMC Bioinform.* **2013**, *14*. [CrossRef] [PubMed]
11. Tas, J.M.J.; Mesin, L.; Pasqual, G.; Targ, S.; Jacobsen, J.T.; Mano, Y.M.; Chen, C.S.; Weill, J.C.; Reynaud, C.A.; Browne, E.P.; et al. Visualizing antibody affinity maturation in germinal centers. *Science* **2016**, *351*, 1048–1054. [CrossRef]
12. Castro, M.; Lythe, G.; Molina-París, C.; Ribeiro, R.M. Mathematics in modern immunology. *Interface Focus* **2016**, *6*, 20150093. [CrossRef] [PubMed]
13. Faro, J.; Castro, M.; Molina-París, C. A unifying mathematical framework for experimental TCR-pMHC kinetic constants. *Sci. Rep.* **2017**, *7*, 46741. [CrossRef] [PubMed]
14. Mason, D.W.; Williams, A.F. The kinetics of antibody binding to membrane antigens in solution and at the cell surface. *Biochem. J.* **1980**, *187*, 1–20. [CrossRef] [PubMed]
15. Williams, A.F. Out of equilibrium. *Nature* **1991**, *352*, 473–474. [CrossRef] [PubMed]
16. Tolar, P.; Hanna, J.; Krueger, P.D.; Pierce, S.K. The Constant Region of the Membrane Immunoglobulin Mediates B cell–receptor Clustering and Signaling in Response to Membrane Antigens. *Immunity* **2009**, *30*, 44–55. [CrossRef]
17. Treanor, B.; Depoil, D.; Gonzalez-Granja, A.; Barral, P.; Weber, M.; Dushek, O.; Bruckbauer, A.; Batista, F.D. The membrane skeleton controls diffusion dynamics and signaling through the B cell receptor. *Immunity* **2010**, *32*, 187–199. [CrossRef] [PubMed]
18. Wan, Z.; Xu, C.; Chen, X.; Xie, H.; Li, Z.; Wang, J.; Ji, X.; Chen, H.; Ji, Q.; Shaheen, S.; et al. PI(4,5)P2 determines the threshold of mechanical force-induced B cell activation. *J. Cell Biol.* **2018**, *217*, 2565–2582. [CrossRef]
19. Cantor, C.R.; Schimmel, P.R. *Biophysical Chemistry Part 2*; Freeman: San Francisco, CA, USA, 1980; p. 584.
20. Saltzman, W.M.; Radomsky, M.L.; Whaley, K.J.; Cone, R.A. Antibody diffusion in human cervical mucus. *Biophys. J.* **1994**, *66*, 508–515. [CrossRef]
21. Stingaciu, L.R.; Ivanova, O.; Ohl, M.; Biehl, R.; Richter, D. Fast antibody fragment motion: Flexible linkers act as entropic spring. *Sci. Rep.* **2016**, *6*, 22148. [CrossRef]
22. Lauffenburger, D.; Linderman, J. *Receptors: Models for Binding, Trafficking, and Signaling*; Oxford University Press: New York, NY, USA, 1996.
23. Reth, M. Matching cellular dimensions with molecular sizes. *Nat. Immunol.* **2013**, *14*, 765. [CrossRef]
24. Wrigley, N.; Brown, E.; Skehel, J. Electron microscopic evidence for the axial rotation and inter-domain flexibility of the fab regions of immunoglobulin G. *J. Mol. Biol.* **1983**, *169*, 771–774. [CrossRef]
25. Wade, R.; Taveau, J.; Lamy, J. Concerning the axial rotational flexibility of the Fab regions of immunoglobulin G. *J. Mol. Biol.* **1989**, *206*, 349–356. [CrossRef]
26. Roux, K.H.; Strelets, L.; Michaelsen, T.E. Flexibility of human IgG subclasses. *J. Immunol.* **1997**, *159*, 3372–3382. Available online: <https://www.jimmunol.org/content/159/7/3372.full.pdf> (accessed on 13 July 2019). [PubMed]
27. Saphire, E.O.; Stanfield, R.L.; Crispin, M.M.; Parren, P.W.; Rudd, P.M.; Dwek, R.A.; Burton, D.R.; Wilson, I.A. Contrasting IgG Structures Reveal Extreme Asymmetry and Flexibility. *J. Mol. Biol.* **2002**, *319*, 9–18. [CrossRef]
28. Løset, G.Å.; Roux, K.H.; Zhu, P.; Michaelsen, T.E.; Sandlie, I. Differential Segmental Flexibility and Reach Dictate the Antigen Binding Mode of Chimeric IgD and IgM: Implications for the Function of the B Cell Receptor. *J. Immunol.* **2004**, *172*, 2925–2934. [CrossRef]
29. Arnold, J.N.; Wormald, M.R.; Sim, R.B.; Rudd, P.M.; Dwek, R.A. The Impact of Glycosylation on the Biological Function and Structure of Human Immunoglobulins. *Annu. Rev. Immunol.* **2007**, *25*, 21–50. [CrossRef] [PubMed]
30. Ramaraj, T.; Angel, T.; Dratz, E.A.; Jesaitis, A.J.; Mumei, B. Antigen–antibody interface properties: Composition, residue interactions, and features of 53 non-redundant structures. *Biochim. Biophys. Acta (BBA)-Proteins Proteom.* **2012**, *1824*, 520–532. [CrossRef]
31. Saini, S.S.; Farrugia, W.; Muthusamy, N.; Ramsland, P.A.; Kaushik, A.K. Structural Evidence for a New IgG1 Antibody Sequence Allele of Cattle. *Scand. J. Immunol.* **2007**, *65*, 32–38. [CrossRef]
32. Torres, M.; Fernández-Fuentes, N.; Fiser, A.; Casadevall, A. The Immunoglobulin Heavy Chain Constant Region Affects Kinetic and Thermodynamic Parameters of Antibody Variable Region Interactions with Antigen. *J. Biol. Chem.* **2007**, *282*, 13917–13927. [CrossRef]
33. Oi, V.T.; Vuong, T.M.; Hardy, R.; Reidler, J.; Dangl, J.; Herzenberg, L.A.; Stryer, L. Correlation between segmental flexibility and effector function of antibodies. *Nature* **1984**, *307*, 136–140. [CrossRef]

34. Hussain, R.; Dawood, G.; Abrar, N.; Toossi, Z.; Minai, A.; Dojki, M.; Ellner, J.J. Selective increases in antibody isotypes and immunoglobulin G subclass responses to secreted antigens in tuberculosis patients and healthy household contacts of the patients. *Clin. Diagn. Lab. Immunol.* **1995**, *2*, 726–732. Available online: <https://cvi.asm.org/content/2/6/726.full.pdf> (accessed on 22 July 2019). [CrossRef]
35. Golding, B. *Cytokine Regulation of Humoral Immune Responses*; Topics in Vaccine Adjuvant Research; CRC Press: Boca Raton, FL, USA, 1991.
36. Hanson, D.C.; Yguerabide, J.; Schumaker, V.N. Segmental flexibility of immunoglobulin G antibody molecules in solution: A new interpretation. *Biochemistry* **1981**, *20*, 6842–6852. [CrossRef]
37. Saffman, P.; Delbrück, M. Brownian motion in biological membranes. *Proc. Natl. Acad. Sci. USA* **1975**, *72*, 3111–3113. [CrossRef]
38. Schlessinger, J. Lateral and rotational diffusion of EGF-receptor complex: Relationship to receptor-mediated endocytosis. *Biopolymers* **1983**, *22*, 347–353. [CrossRef] [PubMed]
39. Hanson, D.C.; Yguerabide, J.; Schumaker, V.N. Rotational dynamics of immunoglobulin G antibodies anchored in protein a soluble complexes. *Mol. Immunol.* **1985**, *22*, 237–244. [CrossRef]
40. Schumaker, V.N.; Phillips, M.L.; Hanson, D.C. Dynamic aspects of antibody structure. *Mol. Immunol.* **1991**, *28*, 1347–1360. [CrossRef]
41. Torres, M.; May, R.; Scharff, M.D.; Casadevall, A. Variable-Region-Identical Antibodies Differing in Isotype Demonstrate Differences in Fine Specificity and Idiotype. *J. Immunol.* **2005**, *174*, 2132–2142. [CrossRef]
42. Szakal, A.; Kosco, M.; Tew, J. A novel in vivo follicular dendritic cell-dependent iccosome-mediated mechanism for delivery of antigen to antigen-processing cells. *J. Immunol.* **1988**, *140*, 341–353. [PubMed]
43. Natkanski, E.; Lee, W.Y.; Mistry, B.; Casal, A.; Molloy, J.E.; Tolar, P. B cells use mechanical energy to discriminate antigen affinities. *Science* **2013**, *340*, 1587–1590. [CrossRef]
44. Nowosad, C.R.; Spillane, K.M.; Tolar, P. Germinal center B cells recognize antigen through a specialized immune synapse architecture. *Nat. Immunol.* **2016**, *17*, 870–877. [CrossRef]
45. Spillane, K.M.; Tolar, P. B cell antigen extraction is regulated by physical properties of antigen-presenting cells. *J. Cell Biol.* **2017**, *216*, 217–230. [CrossRef]
46. Wang, J.; Lin, F.; Wan, Z.; Sun, X.; Lu, Y.; Huang, J.; Wang, F.; Zeng, Y.; Chen, Y.H.; Shi, Y.; et al. Profiling the origin, dynamics, and function of traction force in B cell activation. *Sci. Signal.* **2018**, *11*. [CrossRef] [PubMed]
47. Suzuki, K.; Grigorova, I.; Phan, T.G.; Kelly, L.M.; Cyster, J.G. Visualizing B cell capture of cognate antigen from follicular dendritic cells. *J. Exp. Med.* **2009**, *206*, 1485–1493. [CrossRef] [PubMed]
48. Pereverzev, Y.V.; Prezhdo, E.; Sokurenko, E.V. The two-pathway model of the biological catch-bond as a limit of the allosteric model. *Biophys. J.* **2011**, *101*, 2026–2036. [CrossRef] [PubMed]
49. Das, D.K.; Feng, Y.; Mallis, R.J.; Li, X.; Keskin, D.B.; Hussey, R.E.; Brady, S.K.; Wang, J.H.; Wagner, G.; Reinherz, E.L.; et al. Force-dependent transition in the T-cell receptor β -subunit allosterically regulates peptide discrimination and pMHC bond lifetime. *Proc. Natl. Acad. Sci. USA* **2015**, *112*, 1517–1522. [CrossRef] [PubMed]
50. Shen, Z.; Liu, S.; Li, X.; Wan, Z.; Mao, Y.; Chen, C.; Liu, W. Conformational change within the extracellular domain of B cell receptor in B cell activation upon antigen binding. *eLife* **2019**, *8*. [CrossRef] [PubMed]
51. Sun, Y.; Estevez, A.; Schlothauer, T.; Wecksler, A.T. Antigen physicochemical properties allosterically effect the IgG Fc-region and Fc neonatal receptor affinity. *mAbs* **2020**, *12*, 1802135. [CrossRef]
52. Qaraghuli, M.M.A.; Kubiak-Ossowska, K.; Ferro, V.A.; Mulheran, P.A. Antibody-protein binding and conformational changes: identifying allosteric signalling pathways to engineer a better effector response. *Sci. Rep.* **2020**, *10*, 13696. [CrossRef]
53. Foote, J.; Milstein, C. Conformational isomerism and the diversity of antibodies. *Proc. Natl. Acad. Sci. USA* **1994**, *91*, 10370–10374. [CrossRef]
54. Fernández-Quintero, M.L.; Pomarici, N.D.; Math, B.A.; Kroell, K.B.; Waibl, F.; Bujotzek, A.; Georges, G.; Liedl, K.R. Antibodies exhibit multiple paratope states influencing VH–VL domain orientations. *Commun. Biol.* **2020**, *3*. [CrossRef] [PubMed]
55. Ju, L.; Dong, J.F.; Cruz, M.A.; Zhu, C. The N-terminal Flanking Region of the A1 Domain Regulates the Force-dependent Binding of von Willebrand Factor to Platelet Glycoprotein. *J. Biol. Chem.* **2013**, *288*, 32289–32301. [CrossRef] [PubMed]
56. Allen, L.J. *An Introduction to Stochastic Processes with Applications to Biology*; CRC Press: Boca Raton, FL, USA, 2010.
57. Turányi, T. Sensitivity analysis of complex kinetic systems. Tools and applications. *J. Math. Chem.* **1990**, *5*, 203–248. [CrossRef]
58. Faro, J.; von Haeften, B.; Gardner, R.; Faro, E. A Sensitivity Analysis Comparison of Three Models for the Dynamics of Germinal Centers. *Front. Immunol.* **2019**, *10*. [CrossRef]
59. Wan, Z.; Zhang, S.; Fan, Y.; Liu, K.; Du, F.; Davey, A.M.; Zhang, H.; Han, W.; Xiong, C.; Liu, W. B cell activation is regulated by the stiffness properties of the substrate presenting the antigens. *J. Immunol.* **2013**, *190*, 4661–4675. [CrossRef]
60. Kwak, K.; Quizon, N.; Sohn, H.; Saniee, A.; Manzella-Lapeira, J.; Holla, P.; Brzostowski, J.; Lu, J.; Xie, H.; Xu, C.; et al. Intrinsic properties of human germinal center B cells set antigen affinity thresholds. *Sci. Immunol.* **2018**, *3*. [CrossRef]
61. Huse, M. Mechanical forces in the immune system. *Nat. Rev. Immunol.* **2017**, *17*, 679–690. [CrossRef]
62. González, C.; Chames, P.; Kerfelec, B.; Baty, D.; Robert, P.; Limozin, L. Nanobody-CD16 Catch Bond Reveals NK Cell Mechanosensitivity. *Biophys. J.* **2019**, *116*, 1516–1526. [CrossRef]
63. Huang, J. TCR-Mediated Internalization of Peptide-MHC Complexes Acquired by T Cells. *Science* **1999**, *286*, 952–954. [CrossRef]
64. Wyman, J. The turning wheel: A study in steady states. *Proc. Natl. Acad. Sci. USA* **1975**, *72*, 3983–3987. [CrossRef]